Composites: Part B 66 (2014) 453–465

Contents lists available at ScienceDirect

Composites: Part B

journal homepage: www.elsevier.com/locate/compositesb

Finite element analysis of free vibration of the delaminated composite plate with variable kinematic multilayered plate elements

S. Keshava Kumar [a,b], M. Cinefra [b,*], E. Carrera [b], Ranjan Ganguli [a], Dineshkumar Harursampath [a]

[a] Department of Aerospace Engineering, Indian Institute of Science, Bangalore, India
[b] Department of Mechanics and Aerospace Engineering, Politecnico di Torino, Torino, Italy

ARTICLE INFO

Article history:
Received 28 February 2014
Received in revised form 21 May 2014
Accepted 29 May 2014
Available online 24 June 2014

Keywords:
A. Layered structures
B. Delamination
C. Finite Element Analysis (FEA)
Plate

ABSTRACT

Composite laminates are prone to delamination. Implementation of delamination in the Carrera Unified Formulation frame work using nine noded quadrilateral MITC9 element is discussed in this article. MITC9 element is devoid of shear locking and membrane locking. Delaminated as well as healthy structure is analyzed for free mode vibration. The results from the present work are compared with the available experimental or/and research article or/and the three dimensional finite element simulations. The effect of different kinds and different percentages of area of delamination on the first three natural frequencies of the structure is discussed. The presence of open-mode delamination mode shape for large delaminations within the first three natural frequencies is discussed. Also, the switching of places between the second bending mode, with that of the first torsional mode frequency is discussed. Results obtained from different ordered theories are compared in the presence of delamination. Advantage of layerwise theories as compared to equivalent single layer theories for very large delaminations is stated. The effect of different kinds of delamination and their effect on the second bending and first torsional mode shape is discussed.

1. Introduction

Composite laminate structures are widely used in aircraft, helicopters, wind turbine blades and in other industries. There are many ways of analyzing laminated structures; a detailed review articles on available methods for the analysis of laminated plates and shells, and its historical development are documented in articles [1,2]. Laminated composite structures are prone to defects such as matrix cracking, strength and stiffness degradation due to aging or corrosion, and delamination between plies [3,4]. Delamination in the composite structure may occur either during the manufacturing process or during service period of the structure [5]. However, delamination in a structure may lead to catastrophic failure of the structure [3,6,7]. Delamination models are required to facilitate the understanding of the effect of the delamination on the structures, and analyze possible algorithms for structural health monitoring of delaminated structures.

Analysis of laminated structures can be carried out using many theories. Available theories of composite laminated plates can be classified into [8,9]:

- Equivalent single layer (ESL) theories.
- Layerwise (LW) theories.
- Continuum-based three dimensional (3D) elasticity theories.

ESL theories can be grouped into axiomatic or asymptotic based theories, depending on the method of derivation [8]. In axiomatic framework, displacement or/and stress in the thickness direction is assumed and the 3D physical problem is collapsed into a two dimensional mathematical problem [8]. Based on the order of displacement approximation in the thickness direction, ESL theories are further classified into Classical Laminated plated Theory (CLT), First order Shear Deformation Theory (FSDT), Higher order Shear Deformation Theories (HSDT), and Zig-Zag (ZZ) theory. In asymptotic based theory, 3D energy terms are expanded in terms small parameters. These small parameters may be geometrical parameters, like ratio of thickness to the wavelength of deformation, maximum allowable strains, or/and material small parameters like shear modulus to Young's modulus ratio. Three dimensional energy terms are expanded as a series in these small

* Corresponding author. Tel.: +39 011 090 6869.
E-mail addresses: keshav@aero.iisc.ernet.in (S. Keshava Kumar), maria.cinefra@polito.it (M. Cinefra), erasmo.carrera@polito.it (E. Carrera), ganguli@aero.iisc.ernet.in (R. Ganguli), dinesh@aero.iisc.ernet.in (D. Harursampath).

http://dx.doi.org/10.1016/j.compositesb.2014.05.031
1359-8368/

parameters and, based on requirements, higher order terms are truncated, in the variational statement [10]. Layerwise theories are kind of quasi 3D theories, though each layer is analyzed using an ESL theory. Again, based on the independent variables chosen, theories can regrouped into displacement-based, stress-based or mixed formulations.

Different refined and advanced shell/plate models are contained in the Carrera's Unified Formulation (CUF). The CUF permits to obtain, in a general and unified manner, several models that can differ by the chosen order of expansion in the thickness direction, by the equivalent single layer or layer wise approach and by the variational statement used [11,12]. By implementing delamination model in the CUF frame-work, analysis of delaminated structures can be carried out using several models.

Finite element implementation of above theories is carried out by many researchers. Finite element implementation of ESL theories can be broadly classified based on:

- shape of element (Triangular or Quadrilateral) [13];
- number of nodes in the element [14];
- degrees of freedom per node [15,9];
- type of interpolation function [16,9]; and
- integration technique [17].

A comprehensive review on the finite element implementation of plate theories is given in the article by [9]. A comparative view on ESL and LW plate theories is give by [18]. Layerwise plate theory is used by many authors and for different application; few of the references for LW plate theories are [19–21]. Trigonometric LW shear deformation theory is implemented by [22]. [23] introduced Zig-Zag (ZZ) plate theory for laminated plates. ZZ plate theory is extended to include higher-order thickness function by [24]. ZZ plate theories are used in many applications, and some examples are given by these articles [25–27].

Delamination in the plates is modeled by many researchers, and delamination modeling can be broadly categorized into (a) the region approach and (b) the layerwise approach [28]. In region-wise approach, delaminated segment is divided into sub-laminates and the continuity conditions are imposed at the junctions of delaminated segments and the healthy segment. In layerwise theories, delamination can be modeled by introducing discontinuity functions in the displacement fields or by adding an additional embedded layer at the interface of delamination [28,29,5]. Delamination models can also be regrouped into free-mode delamination models and constrained-mode delamination models [28]. In free-mode delamination models, the sub-laminates of the delaminated segments are allowed to move independently without touching each other. Free-mode delamination model leads to non-physical displacement modes. Constrained-mode delamination models will not allow such non-physical displacement modes. Constrained-mode delamination models impose penalty conditions on the delaminated sub-laminates, by restricting the sub-laminates to move together. However, this option would not simulate the open-mode deformation conditions. This led to further enhancement of the constrained-mode delamination model by incorporating nonlinear springs in between the delaminated sub-laminates. A detailed review and historical development of delamination models is given by authors Della and Shu [28]. Delamination models are implemented in ZZ theories by [25], and by [30].

The present article uses Mixed Interpolation Tensorial Component, nine node quadrilateral (MITC9) element for the laminated plate analysis. MITC9 element is devoid of shear and membrane locking phenomenon [31]. Delamination model has been implemented in CUF frame-work. Results for the first few natural frequencies and modeshapes of the structure are obtained using CUF plate code for healthy as well as delaminated plate. Results are compared with existing literature or with 3D finite element simulation. The major contribution of the present article is the implementation of the delamination model in the CUF frame-work. The results for the delaminated plates for higher order theories, other than those presented in the literature are tabulated.

2. Variable kinematic model via Carrera Unified Formulation

Carrera Unified Formulation (CUF) is a technique which handles a large variety of bi-dimensional models in an unified manner. According to CUF, the governing equations are written in terms of few fundamental nuclei which do not formally depend on the order of expansion N used in the z direction and on the description of variables: ESL or LW. The application of a two-dimensional method for plates permits to express the unknown variables as a set of thickness functions depending only on the thickness coordinate z and the corresponding variables depending on the in plane coordinates x and y. So that, a generic variable, for instance the displacement $u(x,y,z)$, and its variation $\delta u(x,y,z)$, are written according to the following general expansion:

$$\begin{aligned}\boldsymbol{u}(x,y,z) &= F_s(z)\boldsymbol{u}_s(x,y), \quad \delta\boldsymbol{u}(x,y,z) \\ &= F_\tau(z)\delta\boldsymbol{u}_\tau(x,y), \quad \text{with} \quad \tau,s = 0,\ldots,N\end{aligned} \tag{1}$$

Bold letters denote arrays and the summing convention with repeated indexes τ and s is assumed. The order of expansion N goes from first to higher-order values and, depending on the used thickness functions, a model can be ESL or LW. If the variable is assumed for the whole multilayer, the approach is ESL and a Taylor expansion is employed as thickness function $F(z)$:

$$\begin{aligned}\boldsymbol{u} = F_0\,\boldsymbol{u}_0 + F_1\,\boldsymbol{u}_1 + \ldots + F_N\,\boldsymbol{u}_N = F_\tau\,\boldsymbol{u}_\tau \text{ with } \tau \\ = 0,1,\ldots,N\end{aligned} \tag{2}$$

$$F_0 = z^0 = 1,\ F_1 = z^1 = z,\ \ldots,\ F_N = z^N \tag{3}$$

When the description is LW the variable is considered independent in each layer:

$$\boldsymbol{u^k} = F_t\,\boldsymbol{u}_t^k + F_b\,\boldsymbol{u}_b^k + F_l\,\boldsymbol{u}_l^k \quad with \quad l = 2,\ldots,N \tag{4}$$

where t and b indicate the top and bottom of the plate and the thickness functions $F(z)$ are combinations of Legendre polynomials:

$$\begin{aligned}P_0 = 1,\ P_1 = \zeta_k,\ P_2 = \frac{(3{\zeta_k}^2 - 1)}{2},\ P_3 = \frac{5{\zeta_k}^3}{2} - \frac{3\zeta_k}{2},\ P_4 \\ = \frac{35{\zeta_k}^4}{8} - \frac{15{\zeta_k}^2}{4} + \frac{3}{8}\end{aligned} \tag{5}$$

$$\begin{aligned}F_t = \frac{P_0 + P_1}{2},\ F_b = \frac{P_0 - P_1}{2},\ F_l = P_l - P_{l-2} \quad with \quad l \\ = 2,\ldots,N\end{aligned} \tag{6}$$

The chosen functions have the following interesting properties:

$$\begin{aligned}&\zeta_k = 1 \ : \ F_t = 1;\ F_b = 0;\ F_l = 0 \quad at\ top \\ &\zeta_k = -1 : \ F_t = 0;\ F_b = 1;\ F_l = 0 \quad at\ bottom\end{aligned} \tag{7}$$

that is the interface values of the variables are considered as unknowns.

It is possible to obtain the FSDT model [32,33] from an ESL theory with first order of expansion, by considering a constant transverse displacement through the thickness. An appropriate application of penalty techniques to shear strains leads to CLT [34].

3. MITC9 plate element

In this section, the derivation of a plate finite element for the analysis of multilayered structures is presented. The element is based on both the ESL, ZZ and LW theories contained in the Unified Formulation. A nine-nodes element is considered. After an overview in scientific literature about the methods that permit to withstand the membrane and shear locking, the MITC technique has been adopted for this element.

3.1. Geometrical relations

Plates are bi-dimensional structures in which one dimension (in general the thickness in z direction) is negligible with respect to the other two in-plane dimensions. Geometry and the reference system are indicated in Fig. 1.

Geometrical relations permit the in-plane $\boldsymbol{\epsilon}_p^k$ and out-plane $\boldsymbol{\epsilon}_n^k$ strains to be expressed in terms of the displacement $\boldsymbol{u}$. The following relations hold:

$$\boldsymbol{\epsilon}_p^k = [\epsilon_{xx}^k, \epsilon_{yy}^k, \epsilon_{xy}^k]^T = \boldsymbol{D}_p\ \boldsymbol{u}^k,\ \ \boldsymbol{\epsilon}_n^k = [\epsilon_{xz}^k, \epsilon_{yz}^k, \epsilon_{zz}^k]^T = \boldsymbol{D}_n\ \boldsymbol{u}^k. \tag{8}$$

The explicit form of the introduced arrays is:

$$\boldsymbol{D}_p = \begin{bmatrix} \partial_x & 0 & 0 \\ 0 & \partial_y & 0 \\ \partial_y & \partial_x & 0 \end{bmatrix}, \quad \boldsymbol{D}_n = \begin{bmatrix} \partial_z & 0 & \partial_x \\ 0 & \partial_z & \partial_y \\ 0 & 0 & \partial_z \end{bmatrix}, \tag{9}$$

3.2. MITC method

Considering a 9-nodes finite element, the displacement components are interpolated on the nodes of the element by means of the Lagrangian shape functions N_i:

$$\delta\boldsymbol{u}_\tau = N_i \delta\boldsymbol{u}_{\tau_i} \quad \boldsymbol{u}_s = N_j \boldsymbol{u}_{s_j} \quad \text{with} \quad i,j = 1,\ldots,9 \tag{10}$$

where $\boldsymbol{u}_{s_j}$ and $\delta\boldsymbol{u}_{\tau_i}$ are the nodal displacements and their virtual variations. Substituting in the geometrical relations (Eq. (8)) one has:

$$\begin{aligned} \boldsymbol{\epsilon}_p &= F_\tau \boldsymbol{D}_p (N_i \boldsymbol{I}) \boldsymbol{u}_{\tau_i} \\ \boldsymbol{\epsilon}_n &= F_\tau \boldsymbol{D}_n (N_i \boldsymbol{I}) \boldsymbol{u}_{\tau_i} \end{aligned} \tag{11}$$

where $\boldsymbol{I}$ is the identity matrix.

Considering the local coordinate system (ξ, η), the MITC plate elements [35,36] are formulated by using, instead of the strain components directly computed from the displacements, an interpolation of these within each element using a specific interpolation strategy for each component. The corresponding interpolation points, called *tying points*, are shown in Fig. 2 for a nine-nodes element. Note that the transverse normal strain ϵ_{zz} is excluded from this procedure and it is directly calculated from the displacements.

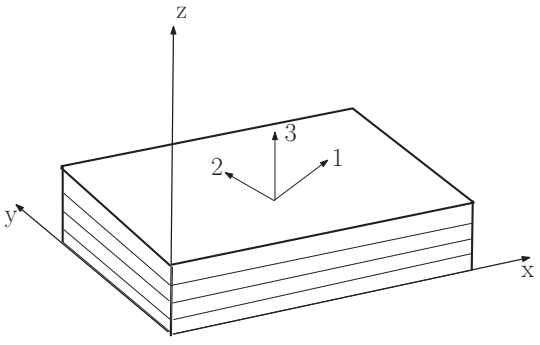

Fig. 1. Reference system of plate.

The interpolating functions are Lagrangian functions and are arranged in the following arrays:

$$\begin{aligned} N_{m1} &= [N_{A1}, N_{B1}, N_{C1}, N_{D1}, N_{E1}, N_{F1}] \\ N_{m2} &= [N_{A2}, N_{B2}, N_{C2}, N_{D2}, N_{E2}, N_{F2}] \\ N_{m3} &= [N_P, N_Q, N_R, N_S] \end{aligned} \tag{12}$$

From this point on, the subscripts $m1, m2$ and $m3$ indicate quantities calculated in the points.

$(A1, B1, C1, D1, E1, F1)$, $(A2, B2, C2, D2, E2, F2)$ and (P, Q, R, S), respectively. Therefore, the strain components are interpolated as follows:

$$\begin{aligned} \boldsymbol{\epsilon}_p &= \begin{bmatrix} \epsilon_{xx} \\ \epsilon_{yy} \\ \epsilon_{yy} \end{bmatrix} = \begin{bmatrix} N_{m1} & 0 & 0 \\ 0 & N_{m2} & 0 \\ 0 & 0 & N_{m3} \end{bmatrix} \begin{bmatrix} \epsilon_{xx_{m1}} \\ \epsilon_{yy_{m2}} \\ \epsilon_{xy_{m3}} \end{bmatrix} \\ \boldsymbol{\epsilon}_n &= \begin{bmatrix} \epsilon_{xz} \\ \epsilon_{yz} \\ \epsilon_{zz} \end{bmatrix} = \begin{bmatrix} N_{m1} & 0 & 0 \\ 0 & N_{m2} & 0 \\ 0 & 0 & 1 \end{bmatrix} \begin{bmatrix} \epsilon_{xz_{m1}} \\ \epsilon_{yz_{m2}} \\ \epsilon_{zz} \end{bmatrix} \end{aligned} \tag{13}$$

where the strains $\epsilon_{xx_{m1}}$, $\epsilon_{yy_{m2}}$, $\epsilon_{xy_{m3}}$, $\epsilon_{xz_{m1}}$, $\epsilon_{yz_{m2}}$ are expressed by means of Eq. (11) in which the shape functions N_i and their derivatives are evaluated in the tying points. For example, one can considers the strain component ϵ_{xx} that is calculated as follows:

$$\begin{aligned} \epsilon_{xx} = {} & N_{A1}\epsilon_{xx_{A1}} + N_{B1}\epsilon_{xx_{B1}} + N_{C1}\epsilon_{xx_{C1}} + N_{D1}\epsilon_{xx_{D1}} + N_{E1}\epsilon_{xx_{E1}} \\ & + N_{F1}\epsilon_{xx_{F1}} \end{aligned} \tag{14}$$

with:

$$\epsilon_{xx_{A1}} = N_{i,x}^{(A1)} F_\tau u_{\tau_i} \tag{15}$$

The superscript $(A1)$ indicates that the shape function and its derivative are evaluated in the point of coordinates $(-\sqrt{\frac{1}{3}}, -\sqrt{\frac{3}{5}})$. Similar expressions can be written for $\epsilon_{xx_{B1}}$, $\epsilon_{xx_{C1}}$, $\epsilon_{xx_{D1}}$, $\epsilon_{xx_{E1}}$, $\epsilon_{xx_{F1}}$.

4. Constitutive equations

The second step towards the governing equations is the definition of the 3D constitutive equations that permit the stresses to be expressed by means of the strains. The generalized Hooke's law is considered, by employing a linear constitutive model for an infinitesimal deformation. In a composite material, these equations are obtained in material coordinates $(1, 2, 3)$ for each orthotropic layer k.

The stress–strain relations are:

$$\begin{aligned} \boldsymbol{\sigma}_p^k &= \boldsymbol{C}_{pp}^k\ \boldsymbol{\epsilon}_p^k + \boldsymbol{C}_{pn}^k\ \boldsymbol{\epsilon}_n^k \\ \boldsymbol{\sigma}_n^k &= \boldsymbol{C}_{np}^k\ \boldsymbol{\epsilon}_p^k + \boldsymbol{C}_{nn}^k\ \boldsymbol{\epsilon}_n^k \end{aligned} \tag{16}$$

where

$$\begin{aligned} \boldsymbol{C}_{pp}^k &= \begin{bmatrix} C_{11}^k & C_{12}^k & C_{16}^k \\ C_{12}^k & C_{22}^k & C_{26}^k \\ C_{16}^k & C_{26}^k & C_{66}^k \end{bmatrix} \quad \boldsymbol{C}_{pn}^k = \begin{bmatrix} 0 & 0 & C_{13}^k \\ 0 & 0 & C_{23}^k \\ 0 & 0 & C_{36}^k \end{bmatrix} \\ \boldsymbol{C}_{np}^k &= \begin{bmatrix} 0 & 0 & 0 \\ 0 & 0 & 0 \\ C_{13}^k & C_{23}^k & C_{36}^k \end{bmatrix} \quad \boldsymbol{C}_{nn}^k = \begin{bmatrix} C_{55}^k & C_{45}^k & 0 \\ C_{45}^k & C_{44}^k & 0 \\ 0 & 0 & C_{33}^k \end{bmatrix} \end{aligned} \tag{17}$$

The material coefficients C_{ij} depend on the Young's moduli E_1, E_2, E_3, the shear moduli G_{12}, G_{13}, G_{23} and Poisson moduli ν_{12}, ν_{13}, ν_{23}, ν_{21}, ν_{31}, ν_{32} that characterize the layer material.

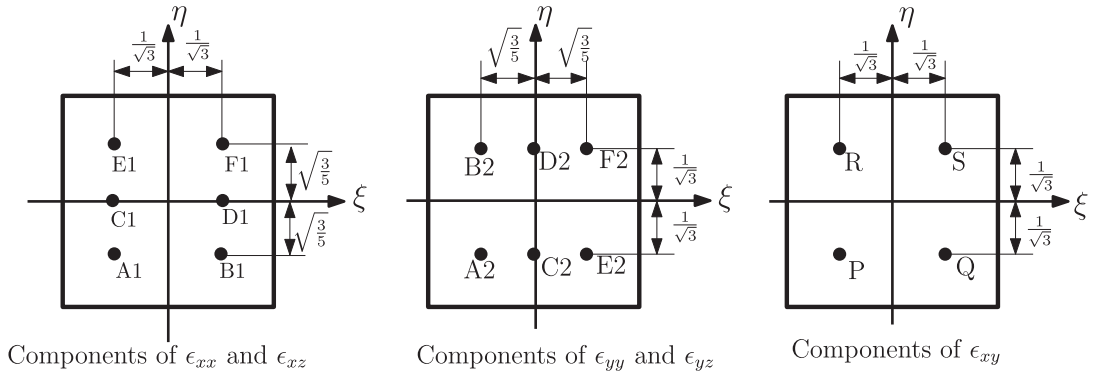

Fig. 2. Tying points for the MITC9 plate element.

5. Governing equations

This section presents the derivation of the governing finite element stiffness matrix and mass matrix based on the Principle of Virtual Displacement (PVD) in the case of multi-layered laminated plates.

The PVD for a multilayered laminated plates is:

$$\int_{\Omega_k}\int_{A_k}\left\{\delta\boldsymbol{\epsilon}_p^{k\,T}\boldsymbol{\sigma}_p^k+\delta\boldsymbol{\epsilon}_n^{k\,T}\boldsymbol{\sigma}_n^k\right\}d\Omega_k\,dz = \int_{\Omega_k}\int_{A_k}\rho^k\delta\mathbf{u}\ddot{\mathbf{u}}\,d\Omega_k\,dz+\int_{\Omega_k}\int_{A_k}\delta\mathbf{u}^k\mathbf{p}^k\,d\Omega_k\,dz \tag{18}$$

where Ω_k and A_k are the integration domains in the plane and in the thickness direction, respectively. The member on the left hand side of the equation represents the variation of the internal work, while the first member on the right hand side of the equation represents the kinetic energy due to inertia and the second member is the external work done due to applied loads. $\boldsymbol{p}^k=\boldsymbol{p}^k(x,y,z)$ is the mechanical load applied to the structure at layer level.

Substituting the constitutive equations (Eq. (16)), the geometrical relations written via the MITC method (Eq. (13)) and applying the Unified Formulation (Eq. (1)) and the FEM approximation (Eq. (10)), one obtains the following governing equations:

$$\delta\boldsymbol{q}_{\tau_i}^k:\quad \boldsymbol{K}^{k\tau sij}\boldsymbol{q}_{s_j}^k=\boldsymbol{M}^{k\tau sij}\ddot{\boldsymbol{q}}_{s_j}^k+\boldsymbol{P}_{\tau_i}^k \tag{19}$$

where $\boldsymbol{K}^{k\tau sij}$ is a 3×3 matrix, called fundamental nucleus, and its explicit expression is given in Appendix A. This is the basic element from which the stiffness matrix of the whole structure is computed. The fundamental nucleus is expanded on the indexes τ and s in order to obtain the stiffness matrix of each layer. Then, the matrices of each layer are assembled at multi-layer level depending on the approach considered, ESL or LW. $\boldsymbol{P}_{\tau i}^k$ is the fundamental nucleus for the external mechanical load. For more details, the reader can refer to [2].

6. Acronyms

Several refined and advanced two-dimensional models are contained in the unified formulation. Depending on the variables description (LW, ESL or ZZ) and the order of expansion N of the displacements in z, a large variety of kinematics plate theories can be obtained. A system of acronyms is given in order to denote these models. The first letter indicates the multi-layer approach which can be equivalent single layer (E) or Layer Wise (L). The number N indicates the order of expansion used in the thickness direction (from 1 to 4). In the case of LW approach, the same order of expansion is used for each layer. In the case of ESL approach, a letter Z can be added if the zig-zag effects of displacements is considered by means of Murakami's zig-zag function. Summarizing, E1–E4 are ESL models. If Murakami zig-zag function is used, these equivalent single layer models are indicated as EZ1–EZ3. In the case of layerwise approaches, the letter L is considered in place of E, so the acronyms are L1–L4. Classical theories such as Classical Lamination Theory (CLT) and First order Shear Deformation Theory (FSDT), can be obtained as particular cases of E1 theory simply imposing constant value of w through the thickness direction. An appropriate application of penalty technique to shear moduli of the material leads to CLT.

7. Incorporating delamination

Delamination in laminate is modeled either using region based approach or layerwise approach [28]. Region based delamination model is generally employed when ESL models are used for the structure analysis, and layerwise delamination model when LW theory is adopted. There are many research articles based on implementation of these delamination models either by analytical or by numerical methods. A detailed review article on the type of implementation using analytical or numerical methods and using region wise delamination or layerwise delamination model is given by Della and shu [28]. CUF model is capable of simulating ESL as well as LW theories. Implementation of delamination model numerically requires modification at the preprocessor stage or at the assembly stage in the CUF frame-work. To implement delamination in ESL theories numerically, major changes to be carried out is at the preprocessing stage. Where as for delamination implementation using LW theories numerically, major changes to be carried out is at the assembly stage.

7.1. Delamination in ESL and ZZ models

Region wise delamination modeling is used for ESL and ZZ theories. Region wise delamination modeling is incorporated by spliting the delaminated structure in span wise direction into delaminated segment and integral segments. In delaminated region, the segments above and below the delamination in the thickness wise direction are modeled as two separate plates; as shown by the top illustration of Fig. 3. There is a shift in the neutral surfaces of these plates in the delaminated region with that of the neutral surface of the integral plate. The shift in the neutral surfaces gives rise to the coupling of in-plane and bending modes of vibration. At the interface of delaminated region and the integral plate, apart from the continuity condition of the transverse displacement, shear force and bending moments, additional conditions of in-plane displacements and forces have to be satisfied. This is accomplished by having a common node at the interface for the integral segment as well as the delaminated segments; as

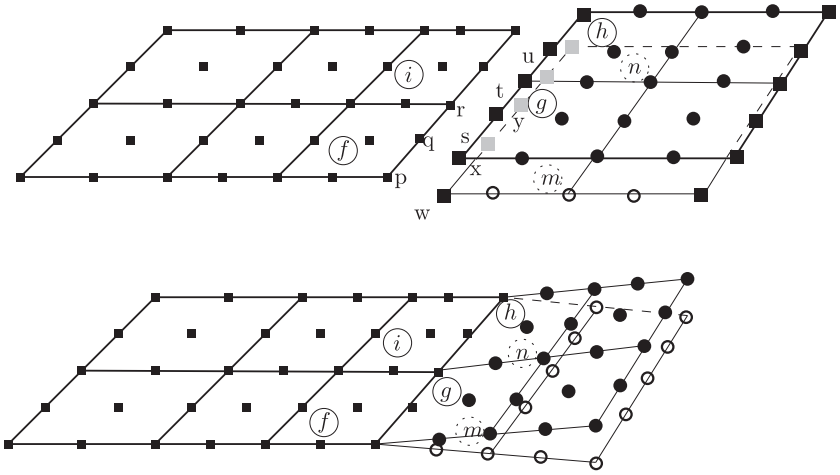

Fig. 3. Delaminated structure mesh representation.

shown by the bottom illustration of Fig. 3. This can be enforced in the finite element context by pacifying the nodal displacements to be same at the interface of integral as well as delaminated segments. To drive this point further, consider the elements f, g, and m, shown in Fig. 3. The nodal displacements for the node p should be same as that of node w and node s, it can be stated mathematically as

$$\boldsymbol{q}_p = \boldsymbol{q}_w = \boldsymbol{q}_s$$

where $\boldsymbol{q}_p$ is the nodal displacement vector of the node p, $\boldsymbol{q}_w$ is the nodal displacement vector for the node w and $\boldsymbol{q}_s$ is the nodal displacement vector for the node s. Similarly the displacement components for the nodes situated at the interface, for elements f, g, m, i, h and n would have the same displacement components. The other way implementing the above condition is by penalty constraint, but having a common node at the interface for integral as well as delaminated segments reduces the number of equations to be solved, and also the implementation can be carried out at the preprocessing stage, which is easier to implement. Differential stretching in the plates above and below delamination plane induces substantial flexural stiffness.

The free mode delamination model is implemented in the present analysis, as in this article emphasis is on free vibration analysis. Constrained mode delamination model can be implemented by adding spring elements, which constrain the transverse displacement of delaminated segments into one another. A nonlinear compressive-only spring, connecting the nodes represented by circle and disk as shown in Fig. 3, has to be used to implement the constrained mode delamination model. This spring hardly influences the stiffness properties of the structure for mode shapes and natural frequency calculations. The spring connecting the disk and circle Fig. 3 is used to represent the contact forces generated between the delaminated segments. Constrained mode model is appropriate while simulating delaminated structures for static and dynamic response analysis, and stability studies. Continuity condition of the displacements is established by having common nodes for the delaminated segments and the integral segment. The eccentricity of the neutral plane of delaminated segments with that of the healthy segments is accounted while calculating cross-sectional stiffness matrices of the laminate.

7.2. Delamination in LW model

Delamination is modeled in layerwise theory either using thin elastic layer concept or by introducing the discontinuity in the displacement functions [28]. Analytically discontinuity in the displacement fields is introduced using Heaviside unit step functions [20]. Finite element wise delamination implementation in LW theory is performed by introducing additional nodes at the location of delaminated region. Schematic of the LW finite element mesh for a delaminated structure is shown in Fig. 4. This is implemented numerically while assembling the element matrix of the delaminated element. This can be stated mathematically as

$$\boldsymbol{q}_{disc} \neq \boldsymbol{q}_{circle}.$$

where $\boldsymbol{q}_{disc}$ is the nodal displacement vector of the node situated at the delamination interface, and $\boldsymbol{q}_{circle}$ is the nodal displacement vector of the node situated at the delamination interface; discs and circles are the nodes as shown in Fig. 4. Schematic of an assembled block matrix for a node, for a healthy as well as delaminated layerwise element, is shown in Fig. 5. Delamination is between layer two and layer three, for the schematic shown in Fig. 5

Block matrices for healthy laminated element are all square in nature, but for the delaminated element block matrices may not be square in nature. Schematic of element matrices of intact as well as delaminated elements is shown in Fig. 6. In the schematic of matrices shown, the nodes 2, 6 and 9 fall in the delaminated region, hence the size of the nodal matrices for these nodes are bigger than those of the nodes falling in the undelaminated location. As a result of this, the off-diagonal block matrices will be rectangular in shape. This method of implementing the delamination is handled at the assembly stage.

8. Numerical results

A laminated composite beam made of graphite/epoxy laminate with stacking sequence $[0/90]_{2s}$, 0.127 m length, 0.0127 m breadth, and 10.16 mm thickness, is considered for the numerical simulation for the healthy as well as delaminated states. Each ply has a thickness of $1.27mm$. The material properties of the lamina are:

- Young's moduli $E_{11} = 134$ GPa and $E_{22} = 10.3$ GPa;
- shear modulus $G_{12} = 5$ GPa;
- Poisson's ratio $v_{12} = 0.33$; and
- material density $\rho = 1480\ \mathrm{kg/m^3}$.

One of the smaller edge of the plate is restrained, and the remaining three edges are free to deform. This beam is modeled using plate elements. This particular configuration is used in simulation, as experimental, analytical and numerical results are

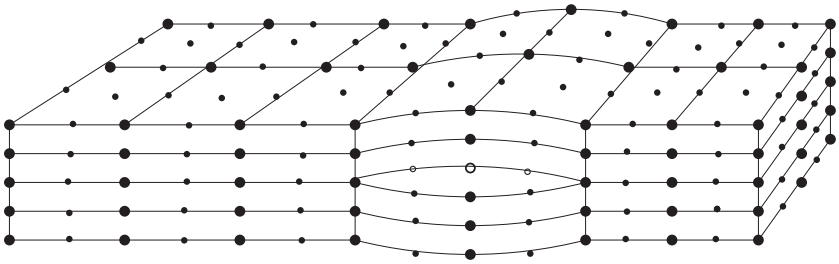

Fig. 4. Schematic of delaminated plate mesh for LW theory.

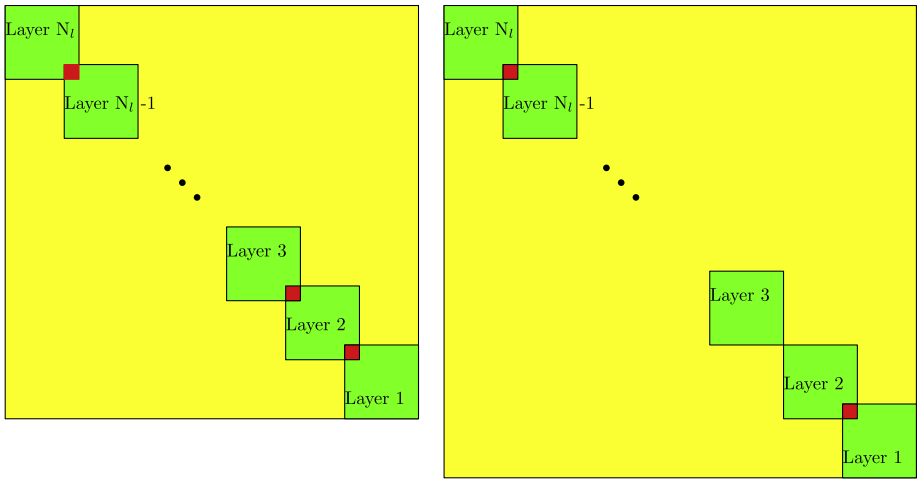

Fig. 5. Schematic of assembly for a node.

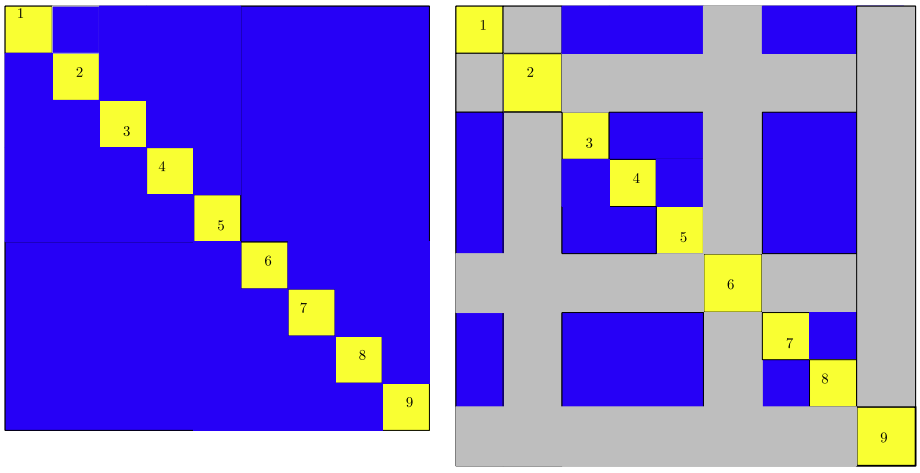

Fig. 6. Schematic of element matrices in LW theory.

available in the literature [28,30,37] for comparison. Results are also validated with 3D finite element simulation using COMSOL 4.2a. The 3D finite element beam model is meshed with 40,000 hexahedral elements. Delamination in the structure is simulated using thin elastic layer.

8.1. Delaminated plate results

First three natural frequencies of healthy, as well as delaminated plate are tabulated in Tables 1–3. Delamination is located at the middle part in the length wise direction of the plate, the length of delamination is 25.4 mm and full width of plate is considered to be delaminated. In the thickness direction delamination is considered at different interfaces, refer to Fig. 7.

The 25.4 mm delamination at any interface has very small effect on the first natural frequency of the structure. This is evident from the results obtained using all theories and also with the experimental results. From the results, it is also evident that the location of delamination in the thickness direction has an impact on the natural frequencies, refer to Table 1. The first mode shape of the beam, delaminated at interface 1, obtained using LW model is shown in Fig. 8. The effect of delamination on the natural frequencies is seen to decrease as the delamination location shifts from interface 1 to interface 4. FSDT results in the CUF frame-work for

Table 1
Comparison of healthy beam results with different theories.

Frequency (Hz)	Healthy beam	Interface 1	Interface 2	Interface 3	Interface 4
Exp [37]	79.88, 79.75, 79.88	78.376, 79.126, 77.001	78.375, 78.375, 76.626	79.625, 80.125, 80.625	75.315, 75.250, 77.250
FSDT [28]	82.04	80.133	81.385	81.461	81.598
3D FEM [3]	81.46	81.43	81.39	81.76	81.37
ED1	81.99	81.21	81.27	81.78	82.23
ED2	82.02	81.28	81.34	81.82	81.84
ED3	82.01	81.22	81.29	81.81	81.83
ED4	82.01	81.22	81.29	81.80	81.82
LD1	82.01	80.98	81.08	81.75	81.78
LD2	81.99	80.96	81.06	81.74	81.77
LD3	81.99	80.96	81.06	81.74	81.77
LD4	81.99	80.96	81.06	81.74	81.77
EDZ1	82.44	81.66	81.73	82.23	NA
EDZ2	82.02	81.27	81.33	81.81	NA
EDZ3	82.01	81.22	81.28	81.80	NA
FSDT	81.99	81.24	81.30	81.80	81.82
CLT	82.02	81.27	81.33	81.83	81.85

Table 2
Comparison of second natural frequency of a healthy beam with different theories.

Frequency (Hz)	Healthy beam	Interface 1	Interface 2	Interface 3	Interface 4
3D FEM	510.97	510.55	509.06	508.89	508.72
ED1	512.86	510.71	510.84	510.72	513.53
ED2	513.09	511.68	511.77	511.44	511.99
ED3	512.79	511.30	511.41	511.12	511.68
ED4	513.11	511.29	511.40	511.10	511.67
LD1	512.82	511.21	511.34	510.52	511.33
LD2	512.76	511.15	511.27	510.45	511.26
LD3	512.76	511.15	511.27	510.45	511.26
LD4	512.76	511.15	511.27	510.45	511.26
EDZ1	515.67	513.54	513.75	513.53	NA
EDZ2	513.06	511.64	511.73	511.41	NA
EDZ3	512.76	511.27	511.38	511.09	NA
FSDT	512.85	511.48	511.57	511.25	511.82
CLT	514.08	512.68	512.78	512.46	513.03

Table 3
Comparison of third natural frequency of a healthy beam with different theories.

Frequency (Hz)	Healthy beam	Interface 1	Interface 2	Interface 3	Interface 4
3D FEM [3]	602.42	548.32	565.92	581.55	589.63
ED1	615.52	561.41	569.77	590.34	590.76
ED2	615.62	561.88	570.77	589.50	603.07
ED3	614.28	558.08	566.93	587.16	600.72
ED4	614.30	557.98	566.83	586.85	600.64
LD1	613.20	555.76	566.35	588.93	604.27
LD2	613.12	555.46	566.06	588.76	604.16
LD3	613.12	555.44	566.04	588.75	604.15
LD4	613.12	555.43	566.035	588.74	604.15
EDZ1	615.77	562.04	570.22	590.76	NA
EDZ2	615.62	561.73	569.83	589.27	NA
EDZ3	614.28	557.88	566.74	586.87	NA
FSDT	611.57	561.59	569.95	590.42	603.38
CLT	619.79	567.42	576.18	597.72	611.27

healthy as well as for delamination location at all the interfaces are almost same as those of the FSDT results from [28]. Results of all the theories are almost all similar in trend for change in delamination location.

Result for the ZZ theory, for the delamination location at interface 4 is stated as NA (Not applicable). ZZ theory is implemented in the framework of ESL theory. In the case of delamination location at interface 4 in the structure, top layer is delaminated from the rest of the laminate. Delamination model in the ESL framework is modeled as individual elements for the top and bottom delaminated segments. The top layer will form a single layer in the delaminated region for the case of delamination at interface 4. For applying ZZ theory in the ESL framework at least two layers are required. Hence, the results for the delamination at interface 4 in the tables are stated as NA.

The second mode natural frequency result obtained from different theories and for delamination location at different interfaces is tabulated in Table 2. The second mode natural frequency result for 25.4 mm length, full width and for delamination location at different interfaces has small change with respect to the healthy beam second mode natural frequency result. The second mode shape of the beam obtained using LW theory is shown in Fig. 9.

It is interesting to note that the natural frequency result for the third mode shape changes with the presence of delamination. The

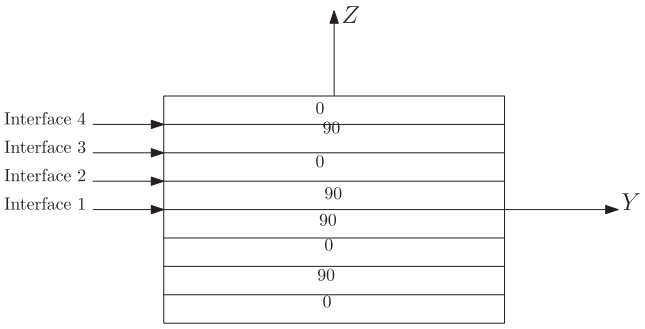

Fig. 7. Delamination considered at different interfaces.

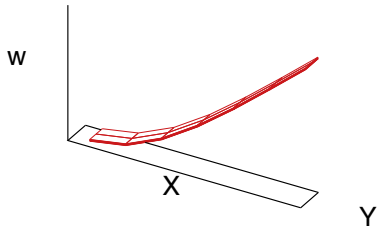

Fig. 8. First mode shape.

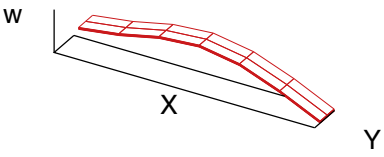

Fig. 9. Second modeshapes.

natural frequency result for third mode shape, for delamination length of 25.4 mm, full width delamination and for delamination location at different interfaces is shown in Table 3. Third mode shape of the beam is plotted in Fig. 10. Third mode shape corresponds to the torsional mode shape of the beam as seen from the plot. Presence of delamination in the beam, has produced a considerable change in the torsional stiffness of the beam and hence the natural frequency of the delaminated beam is much lower than that of the healthy beam, in particular considering the first two bending mode natural frequencies. From the table it is also evident that, as the delamination location shifts from interface 1 to interface 4, the change in natural frequency reduces. Torsional stiffness of the beam has reduced drastically for delamination location at interface 1, but the cross section at the delaminated region gets torsionally stiffer as the delamination location shifts from interface 1 to interface 4.

8.2. Partial delamination in widthwise results

Effect of partial delamination in the width of the structure on the natural frequencies is evaluated. Two cases of partial delaminations

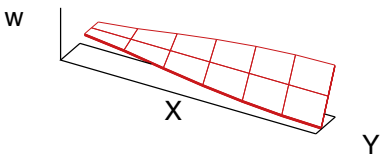

Fig. 10. Third mode shape of the beam.

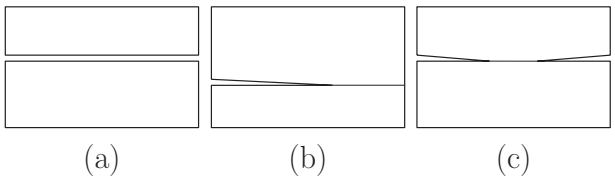

Fig. 11. Width wise delamination cases.

are considered in the simulation, C-type or the Channel type delamination in the cross-section as shown in Fig. 11(b), and I-type delamination in the cross-section as shown in Fig. 11(c).

8.3. C-type, 76.2 mm length delamination

First three natural frequencies for a C-type delaminated structure are tabulated in Tables 4–6. The delamination length of 76.2 mm, different percentage of width delamination and in thickness direction delamination is considered at interface 1. From Table 4, the first bending frequency results obtained using different order theories are quite similar, for different percentages of delamination area. There is a drastic decrease in the natural frequency for the case of full width delamination compared to healthy and other percentages of width delamination.

The second bending frequency of the structure is given in Table 5. The second natural frequency for the partial delamination in the width does not correspond to pure bending mode. The second and third modes for 76.2 mm long delamination and with

Table 4
First bending frequency for 76.2 mm of length and different percentage of width delaminations.

Frequency (Hz)	Healthy beam	50%	70%	Full width
Exp [37]	79.88, 79.75, 79.88	NULL	NULL	68.25, 66.25, 66.38
3D FEM [3]	81.46	80.92	79.83	67.37
ED1	81.99	81.22	78.12	65.99
ED2	82.01	81.30	78.23	66.08
ED3	82.01	81.28	78.13	65.73
ED4	82.01	81.28	78.11	65.64
LD1	82.01	81.25	79.87	67.44
LD2	81.99	81.24	79.86	67.41
LD3	81.99	81.24	79.84	68.02
LD4	81.99	81.24	79.84	68.02
EDZ1	82.44	81.66	78.53	66.35
EDZ2	82.02	81.30	78.22	66.06
EDZ3	82.01	81.30	78.12	65.71
FSDT	81.99	81.27	79.96	66.08
CLT	82.02	81.33	80.06	66.26

Table 5
Second bending frequency for 76.2 mm of length and different percentage of width delaminations.

Frequency (Hz)	Healthy beam	50%	70%	Full width
3D FEM	510.97	495.92	464.59	434.99
ED1	512.86	496.44	455.33	457.68
ED2	513.09	497.17	455.06	456.15
ED3	512.79	496.28	447.44	448.01
ED4	513.11	496.24	443.92	444.59
LD1	512.82	495.32	468.35	415.40
LD2	512.76	495.20	465.33	415.17
LD3	512.76	495.20	465.33	415.17
LD4	512.76	495.20	465.76	415.17
EDZ1	515.67	498.73	471.80	458.42
EDZ2	513.06	497.16	470.85	455.58
EDZ3	512.76	496.20	468.80	447.35
FSDT	512.85	496.98	469.95	457.95
CLT	514.08	499.19	474.67	463.22

Table 6
First torsional frequency for 76.2 mm of length and different percentage of width delaminations.

Frequency (Hz)	Healthy beam	50%	70%	Full width
3D FEM [3]	602.42	528.77	519.96	381.62
ED1	615.52	534.15	486.99	413.47
ED2	614.62	534.40	487.56	411.58
ED3	614.28	532.10	486.06	408.94
ED4	614.30	532.07	485.40	406.66
LD1	613.20	530.16	506.81	391.28
LD2	613.12	517.52	506.66	391.09
LD3	613.12	517.52	506.28	391.08
LD4	613.12	517.52	506.66	391.08
EDZ1	615.77	534.76	489.39	415.58
EDZ2	615.62	534.30	487.40	410.93
EDZ3	614.28	531.97	485.87	408.22
FSDT	611.57	534.28	510.47	414.07
CLT	619.79	540.88	517.01	420.88

partial-width delamination corresponds to bending-twist coupled mode. The full width delamination second mode corresponds to the first torsional mode and the third mode corresponds to the second bending mode. Results for the second bending mode of the present table are comparable with the results presented in the article by Oh et.al [30], but the article only presents full width and healthy plate results. Again from the results of the full width delamination, it is quite evident that the stiffness degradation is maximum for the full width delamination compared to partial delamination.

First torsional mode frequency of the delaminated structure is tabulated in Table 6. First torsional mode corresponds to third natural mode of the healthy structure. In the presence of partial delamination, torsional mode is not purely torsional but bending-twist coupled mode. Presence of full width delamination and 76.2 mm length of delamination results in torsionally weak structure and hence the second mode frequency in the full width delaminated structure corresponds to torsional mode shape. The results of the all the theories in comparison with the 3D FEM simulation are similar for the partial width delamination. Where as, the frequency results from ESL and ZZ theories for the full width delamination case are slightly higher than the LW and 3D FEM results, for the second and third mode frequencies.

8.4. C-type, 101.6 mm length delamination

First three natural frequencies for C-type delamination, for the length of delamination equal to 101.6 mm, and different percentages of the width delamination are tabulated in Tables 7–9. Delamination is considered at the interface 1 in the thickness direction.

Table 7
First natural frequency for 101.6 mm of length and different percentage of width delaminations.

Frequency (Hz)	Healthy beam	50%	70%	Full width
Exp [37]	79.88, 79.75, 79.88			57.62, 57.5, 57.5
3D FEM [3]	81.46	80.32	78.98	55.78
ED1	81.99	79.73	78.24	57.53
ED2	82.01	79.84	78.36	57.45
ED3	82.01	79.78	78.25	57.03
ED4	82.01	80.99	78.22	56.95
LD1	82.01	80.94	78.95	56.67
LD2	81.99	80.96	78.94	57.43
LD3	81.99	80.96	78.94	57.43
LD4	81.99	80.96	78.91	57.43
EDZ1	82.44	80.16	78.52	57.83
EDZ2	82.02	79.84	78.22	57.41
EDZ3	82.01	79.78	78.12	56.98
FSDT	81.99	81.00	79.05	59.64
CLT	82.02	81.06	79.19	59.90

Table 8
Second bending mode frequency for 101.6 mm of length and different percentage of width delaminations.

Frequency (Hz)	Healthy beam	50%	70%	Full width
3D FEM	510.97	462.30	407.29	323.93
ED1	512.86	473.57	425.45	356.29
ED2	513.09	474.08	425.99	355.09
ED3	512.79	472.69	423.88	352.27
ED4	513.11	472.64	423.81	348.78
LD1	512.82	468.15	421.75	322.98
LD2	512.76	471.12	421.55	322.75
LD3	512.76	471.11	421.54	322.74
LD4	512.76	471.11	421.03	322.74
EDZ1	515.67	475.10	455.82	358.20
EDZ2	513.06	474.00	454.76	354.52
EDZ3	512.76	472.58	447.00	351.60
FSDT	512.85	473.92	425.81	356.80
CLT	514.08	477.39	431.29	361.88

Table 9
First torsional mode frequency for 101.6 mm of length and different percentage of width delaminations.

Frequency (Hz)	Healthy beam	50%	70%	Full width
3D FEM [3]	602.42	515.25	487.14	346.76
ED1	615.52	520.37	493.13	422.78
ED2	614.62	520.72	493.65	420.71
ED3	614.28	519.06	491.63	411.24
ED4	614.30	519.04	491.60	404.88
LD1	613.20	514.26	489.94	345.09
LD2	613.12	517.52	489.80	344.95
LD3	613.12	517.52	489.39	344.95
LD4	613.12	517.52	489.39	344.95
EDZ1	615.77	521.45	489.39	423.47
EDZ2	615.62	520.64	487.40	420.07
EDZ3	614.28	518.96	485.87	410.40
FSDT	611.57	520.60	493.49	423.03
CLT	619.79	525.68	499.68	428.64

The first bending mode frequency across the theories is almost all same, refer to Table 7. The results are quite comparable with the experimental and also the 3D FEM simulation.

The results for second bending mode are tabulated in Table 8. Results from different theories are quite comparable with the 3D FEM simulations and also with the results presented in article by Oh et al. [30] for healthy as well as for partial delamination results. Due to long delamination in the beam, there is an additional mode shape very close to the second bending mode shape of the structure. The natural frequency of the traditional second bending mode is 318.81 Hz. This frequency is very close to the opening mode shape (refer to Fig. 12) frequency, and hence the ESL theories fail to capture either the second bending mode shape or the opening mode shape of the structure. 3D FEM simulation and the LW theories alone capture this mode shapes.

First torsional mode corresponds to the third mode or the fourth mode depending on the type of theory we are using, as ESL theories could not capture either the opening mode shape or the second bending mode shape of the structure. The torsional frequency result obtained using CUF LW formulation is almost same as that of the 3D FEM, the ESL theories results are quite higher than the LW and 3D simulations; a trend also seen in the previous results.

From the result tables it is quite evident that the results from the LW theory are quite comparable with the 3D FEM, experimental and also with results from other theories presented by Oh et al. [30]. The results obtained using ESL theories for higher mode shapes, are on the higher side than the 3D FEM simulations and the LW theory, but the same trend is also seen in the results published by Oh et al. [30].

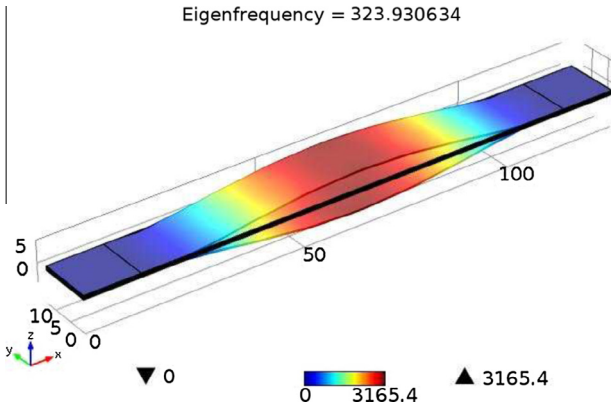

Fig. 12. Open mode delamination.

Table 11
Second bending frequency for 76.2 mm of length and different percentage of width delaminations.

Frequency (Hz)	Healthy beam	50%	70%	Full width
3D FEM	510.97	494.53	483.97	434.99
ED1	512.86	508.79	504.12	457.68
ED2	513.09	509.66	505.23	456.15
ED3	512.79	509.17	504.62	448.01
ED4	513.11	509.16	504.60	444.59
LD1	512.82	508.72	504.05	415.40
LD2	512.76	508.64	503.97	415.17
LD3	512.76	508.64	503.97	415.17
LD4	512.76	508.64	503.96	415.17
EDZ1	515.67	511.53	506.80	458.42
EDZ2	513.06	509.62	505.18	455.58
EDZ3	512.76	509.13	504.57	447.35
FSDT	512.85	509.47	505.04	457.95
CLT	514.08	511.05	506.84	463.22

8.5. I type, 76.2 mm long delamination

Symmetric I type delamination (refer Fig. 11) is considered for the simulation. First three natural frequencies for a I-type delaminated structure are tabulated in Tables 4–6. The delamination length of 76.2 mm, different percentages of width delamination and in thickness direction delamination are considered at interface 1. From Table 10, the first bending frequency results obtained using different order theories are quite similar, for different percentages of delamination area. There is a drastic decrease in the natural frequency for the case of full width delamination compared to healthy and other percentages of delamination.

The second natural frequency result for the I-type delamination is tabulated in Table 11. The same trend of the C-type delamination is seen, but the result for partial delamination is not bending-twist coupled mode shape, it is pure second bending mode shape. Pure second bending mode shape is observed as a result of having symmetric I type delamination, if the I-type delamination was unsymmetrical then the second mode shape for the partial delamination may not be pure bending mode shape. The second bending mode shape frequency for the different partial I-type delamination case (Table 11) are higher in comparison for the same area C-type partial delamination (Table 5).

The third natural frequency or the first torsional frequency of the structure is tabulated in Table 12. Pure torsional mode shape is observed for the partial delamination cases rather than the bending-twist mode shape as observed for C-type delamination. The comparative plots for 76.2 mm delamination and 70% width delamination are shown in Figs. 13 and 14. The torsional frequency of the I-type delamination, for the same percentage of delamination, is lower than that of the C-type delamination.

8.6. I type, 101.6 mm long delamination

First three natural frequencies for symmetric I-type delamination, for the length of delamination equal to 101.6 mm, and different percentages of the width delamination are tabulated in Tables 7–9. Delamination is considered at the interface 1 in the thickness direction. The first bending mode frequency across the theories is almost the same, refer to Table 13. The results are quite comparable with the experimental and 3D FEM simulations.

Second bending natural frequency result for the 101.6 mm length delamination and different percentages of delamination in the width wise case is tabulated in Table 14. The results across the theories are quite similar. The second bending modes are pure bending modes rather than the bending-twist mode as seen for the C-type delamination. The second bending mode frequency for I type delamination is higher than the second bending mode frequency for the C-type delamination, as seen from Tables 8 and 14. In the case of C-type delamination, the second mode is bending-twist coupled mode and hence the second mode frequency for the C-type delamination is lower than that of the I-type delamination, though both the cases have the same percentage of delamination.

First torsional mode shape frequency for the 101.6 mm long delamination at interface 1, and for different percentages of delamination is tabulated in Table 15. The trend of frequency decreases as the increase in delamination, as expected, is also seen in this

Table 10
First natural frequency for 76.2 mm of length and different percentage of width delaminations.

Frequency (Hz)	Healthy beam	50%	70%	Full width
Exp [37]	79.88, 79.75, 79.88			68.25, 66.25, 66.38
3D FEM [3]	81.46	81.12	80.31	67.37
ED1	81.99	81.68	81.31	65.99
ED2	82.01	81.81	81.47	66.08
ED3	82.01	81.79	81.46	65.73
ED4	82.01	81.79	81.60	65.73
LD1	82.01	81.83	81.43	67.44
LD2	81.99	81.82	81.43	67.41
LD3	81.99	81.82	81.43	68.02
LD4	81.99	81.82	81.43	68.02
EDZ1	82.44	82.12	81.45	66.35
EDZ2	82.02	81.80	81.48	66.06
EDZ3	82.01	81.78	81.45	65.71
FSDT	81.99	81.83	81.59	66.08
CLT	82.02	81.87	81.65	66.26

Table 12
First torsional frequency for 76.2 mm of length and different percentage of width delaminations.

Frequency (Hz)	Healthy beam	50%	70%	Full width
3D FEM [3]	602.42	523.51	468.23	381.62
ED1	615.52	518.69	473.81	413.47
ED2	614.62	518.78	473.97	411.58
ED3	614.28	515.60	470.87	408.94
ED4	614.30	515.55	470.80	406.66
LD1	613.20	512.86	468.05	391.28
LD2	613.12	512.60	467.78	391.09
LD3	613.12	512.60	467.78	391.08
LD4	613.12	512.60	467.78	391.08
EDZ1	615.77	518.67	473.82	415.58
EDZ2	615.62	518.52	473.68	410.93
EDZ3	614.28	515.28	470.51	408.22
FSDT	611.57	518.72	473.88	414.07
CLT	619.79	528.44	481.88	420.88

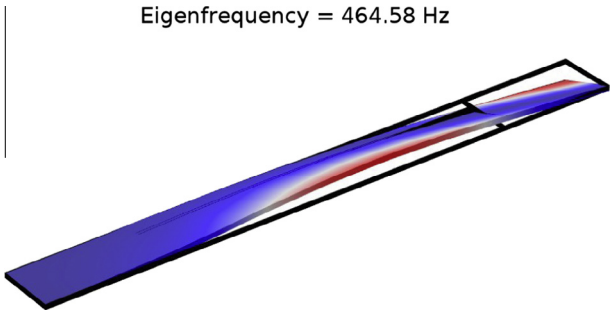

Fig. 13. 76.2 mm long, 70% wide, C type delamination.

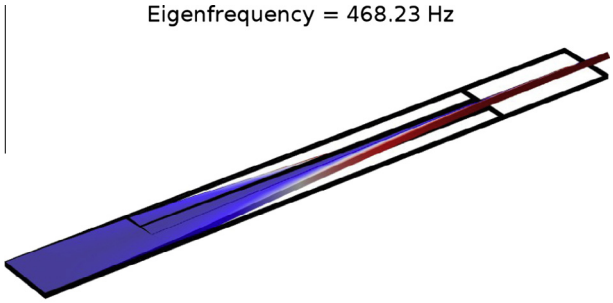

Fig. 14. 76.2 mm long, 70% wide, I type delamination.

Table 13
First natural frequency for 101.6 mm of length and different percentage of width delaminations.

Frequency (Hz)	Healthy beam	50%	70%	Full width
Exp [37]	79.88, 79.75, 79.88	NULL	NULL	57.62, 57.5, 57.5
3D FEM [3]	81.46	80.09	78.04	55.78
ED1	81.99	81.68	81.31	57.53
ED2	82.01	81.81	81.49	57.45
ED3	82.01	81.79	81.46	57.03
ED4	82.01	81.79	81.46	56.95
LD1	82.01	81.77	81.43	56.67
LD2	81.99	81.76	81.43	57.43
LD3	81.99	81.76	81.42	57.43
LD4	81.99	81.76	81.42	57.43
EDZ1	82.44	82.12	81.76	57.83
EDZ2	82.02	81.80	81.48	57.41
EDZ3	82.01	81.78	81.45	56.98
FSDT	81.99	81.78	81.46	59.64
CLT	82.02	81.83	81.52	59.90

Table 14
Second natural frequency for 101.6 mm of length and different percentage of width delaminations.

Frequency (Hz)	Healthy beam	50%	70%	Full width
3D FEM	510.97	473.63	400.37	323.93
ED1	512.86	495.48	438.30	356.29
ED2	513.09	495.54	441.24	355.09
ED3	512.79	492.54	438.47	352.27
ED4	513.11	492.48	438.39	348.78
LD1	512.82	489.89	435.90	322.98
LD2	512.76	489.61	435.61	322.74
LD3	512.76	489.61	435.61	322.74
LD4	512.76	489.61	435.61	322.74
EDZ1	515.67	495.38	441.05	358.20
EDZ2	513.06	495.26	440.94	354.52
EDZ3	512.76	492.18	438.09	351.60
FSDT	512.85	495.50	441.19	356.80
CLT	514.08	504.35	448.53	361.88

Table 15
First torsional frequency for 101.6 mm of length and different percentage of width delaminations.

Frequency (Hz)	Healthy beam	50%	70%	Full width
3D FEM [3]	602.42	493.95	460.80	346.76
ED1	615.52	505.56	496.04	422.78
ED2	614.62	506.43	497.32	420.71
ED3	614.28	505.80	496.48	411.24
ED4	614.30	505.78	496.46	404.88
LD1	613.20	505.23	495.47	345.09
LD2	613.12	505.14	495.62	344.95
LD3	613.12	505.14	495.62	344.95
LD4	613.12	505.14	495.62	344.95
EDZ1	615.77	508.21	498.75	423.47
EDZ2	615.62	506.39	497.26	420.07
EDZ3	614.28	505.75	496.42	410.40
FSDT	611.57	506.24	497.13	423.03
CLT	619.79	508.17	499.48	428.64

table along the expected lines. The torsional mode shape is a pure torsional mode shape for the partial delamination case. The torsional mode frequency for the I-type partial delamination is lower than the torsional mode frequency of the C-type delamination, though both types of delamination have the same percentage of delamination. It is clear that I-type delamination is torsionally weak compared to the C-type delamination, for the same area of delamination in the structure.

9. Conclusion

Implementation of delamination model in the CUF framework for MITC9 quadrilateral element is discussed. The implementation process for ESL and LW theories is explained along with the schematic. The changes in the matrix dimension and shape for the delaminated element in the case of LW theory is discussed with schematics for an example case. The results obtained from the simulation is compared with the existing experimental/literature/3D FEM simulations. The results obtained are quite satisfactory and they match very well with the available results in the research repertoire. The first three natural frequencies obtained using LW theories match very well with the 3D finite element simulations, in comparison with the ESL theories. Layerwise theory is better at handling open mode shapes, which exists for the structures with large delamination; than the ESL theories. The presence of large delamination shifts second and third mode shapes, or rather a new mode shape arises between the first and second mode shapes. The presence of delamination at higher interfaces (refer to Fig. 7) has slightly less impact when compared to the presence of delamination closer to the midsurface of the structure. The presence of C-type partial delamination in the structure will result in bending-twist coupled mode shapes, where as the same is not seen for the symmetric I-type delaminated structures. Symmetric I-type delaminations are stiffer in bending, in comparison with the C-type delaminated structure, if both the structures have the same delaminated area. C-type delaminated structures are stiffer in torsion, in comparison with the I-type delaminated structure, though if both the structures have delaminated area. The advantage of the present formulation technique is that the MITC element is devoid of shear locking and membrane locking. Implementation of delamination in the CUF framework has the advantage of obtaining results for the delaminated structure with wide variety of theories and also different ordered theories.

Acknowledgement

First author would like to thank "Heritage Erasmus Mundus" for the student exchange fellowship.

Appendix A

In order to write the fundamental nucleus $\boldsymbol{K}^{k\tau sij}$ in compact form, the following integrals in the domain Ω_k are defined:

$$\left(W^k_{m1n1};\ W^k_{m1n2};\ W^k_{m2n1};\ W^k_{m2n2}\right) = \int_{\Omega_k} \left(N_{m1}N_{n1};\ N_{m1}N_{n2};\ N_{m2}N_{n1};\ N_{m2}N_{n2}\right) dx_k\, dy_k \tag{20}$$

$$\left(W^k_{m1n3};\ W^k_{m3n1};\ W^k_{m3n3};\ W^k_{m2n3};\ W^k_{m3n2}\right) = \int_{\Omega_k} \left(N_{m1}N_{n3};\ N_{m3}N_{n1};\ N_{m3}N_{n3};\ N_{m2}N_{n3};\ N_{m3}N_{n2}\right) dx_k\, dy_k \tag{21}$$

$$\left(W^k_{m1j};\ W^k_{m2j};\ W^k_{m3j}\right) = \int_{\Omega_k} \left(N_{m1}N_j;\ N_{m2}N_j;\ N_{m3}N_j\right) dx_k\, dy_k \tag{22}$$

$$\left(W^k_{in1};\ W^k_{in2};\ W^k_{in3};\ W^k_{ij}\right) = \int_{\Omega_k} \left(N_iN_{n1};\ N_iN_{n2};\ N_iN_{n3};\ N_iN_j\right) dx_k\, dy_k \tag{23}$$

$$\left(W^k_{m1j_{,x}};\ W^k_{m1j_{,y}};\ W^k_{m2j_{,x}};\ W^k_{m2j_{,y}}\right) = \int_{\Omega_k} \left(N_{m1}\frac{\partial N_j}{\partial x};\ N_{m1}\frac{\partial N_j}{\partial y};\ N_{m2}\frac{\partial N_j}{\partial x};\ N_{m2}\frac{\partial N_j}{\partial y}\right) dx_k\, dy_k \tag{24}$$

$$\left(W^k_{i_{,x}n1};\ W^k_{i_{,y}n1};\ W^k_{i_{,x}n2};\ W^k_{i_{,y}n2}\right) = \int_{\Omega_k} \left(\frac{\partial N_i}{\partial x}N_{n1};\ \frac{\partial N_i}{\partial y}N_{n1};\ \frac{\partial N_i}{\partial x}N_{n2};\ \frac{\partial N_i}{\partial y}N_{n2}\right) dx_k\, dy_k \tag{25}$$

Moreover, the integrals on the domain A_k, in the thickness direction, are written as:

$$J^{k\tau s} = \int_{A_k} F_\tau F_s\, dz \tag{26}$$

$$J^{k\tau_z s} = \int_{A_k} \frac{\partial F_\tau}{\partial z} F_s\, dz \tag{27}$$

$$J^{k\tau s_z} = \int_{A_k} F_\tau \frac{\partial F_s}{\partial z}\, dz \tag{28}$$

$$J^{k\tau_z s_z} = \int_{A_k} \frac{\partial F_\tau}{\partial z}\frac{\partial F_s}{\partial z}\, dz \tag{29}$$

The fundamental nucleus $\boldsymbol{K}^{k\tau sij}$ is a (3×3) matrix and the explicit expression of its components is:

$$K^{k\tau sij}_{xx} = C^k_{55}N^{(m1)}_i N^{(n1)}_j W^k_{m1n1}J^{k\tau_z s_z} + C^k_{66}N^{(m3)}_{i,y}N^{(n3)}_{j,y}W^k_{m3n3}J^{k\tau s} + C^k_{16}N^{(m1)}_{i,x}N^{(n3)}_{j,y}W^k_{m1n3}J^{k\tau s} + C^k_{16}N^{(m3)}_{i,y}N^{(n1)}_{j,x}W^k_{m3n1}J^{k\tau s} + C^k_{11}N^{(m1)}_{i,x}N^{(n1)}_{j,x}W^k_{m1n1}J^{k\tau s} \tag{30}$$

$$K^{k\tau sij}_{xy} = C^k_{45}N^{(m1)}_i N^{(n2)}_{j,y} W^k_{m1n2}J^{k\tau_z s_z} + C^k_{26}N^{(m3)}_{i,y}N^{(n2)}_{j,y}W^k_{m3n2}J^{k\tau s} + C^k_{12}N^{(m1)}_{i,x}N^{(n2)}_{j,y}W^k_{m1n2}J^{k\tau s} + C^k_{66}N^{(m3)}_{i,y}N^{(n3)}_{j,x}W^k_{m3n3}J^{k\tau s} + C^k_{16}N^{(m1)}_{i,x}N^{(n3)}_{j,x}W^k_{m1n3}J^{k\tau s} \tag{31}$$

$$K^{k\tau sij}_{xz} = C^k_{45}N^{(m1)}_i N^{(n2)}_{j,y} W^k_{m1n2}J^{k\tau_z s} + C^k_{55}N^{(m1)}_i N^{(n1)}_{j,x} W^k_{m1n1}J^{k\tau_z s} + C^k_{36}N^{(m3)}_{i,y}W^k_{m3j}J^{k\tau s_z} + C^k_{13}N^{(m1)}_{i,x}W^k_{m1j}J^{k\tau s_z} \tag{32}$$

$$K^{k\tau sij}_{yx} = C^k_{45}N^{(m2)}_i N^{(n1)}_j W^k_{m2n1}J^{k\tau_z s_z} + C^k_{26}N^{(m2)}_{i,y}N^{(n3)}_{j,y}W^k_{m2n3}J^{k\tau s} + C^k_{66}N^{(m3)}_{i,x}N^{(n3)}_{j,y}W^k_{m3n3}J^{k\tau s} + C^k_{12}N^{(m2)}_{i,y}N^{(n1)}_{j,x}W^k_{m2n1}J^{k\tau s} + C^k_{16}N^{(m3)}_{i,x}N^{(n1)}_{j,x}W^k_{m3n1}J^{k\tau s} \tag{33}$$

$$K^{k\tau sij}_{yy} = C^k_{44}N^{(m2)}_i N^{(n2)}_j W^k_{m2n2}J^{k\tau_z s_z} + C^k_{22}N^{(m2)}_{i,y}N^{(n2)}_{j,y}W^k_{m2n2}J^{k\tau s} + C^k_{26}N^{(m3)}_{i,x}N^{(n2)}_{j,y}W^k_{m3n2}J^{k\tau s} + C^k_{26}N^{(m2)}_{i,y}N^{(n3)}_{j,x}W^k_{m2n3}J^{k\tau s} + C^k_{66}N^{(m3)}_{i,x}N^{(n3)}_{j,x}W^k_{m3n3}J^{k\tau s} \tag{34}$$

$$K^{k\tau sij}_{yz} = C^k_{44}N^{(m2)}_i N^{(n2)}_{j,y} W^k_{m2n2}J^{k\tau_z s} + C^k_{45}N^{(m2)}_i N^{(n1)}_{j,x} W^k_{m2n1}J^{k\tau_z s} + C^k_{23}N^{(m2)}_{i,y}W^k_{m2j}J^{k\tau s_z} + C^k_{36}N^{(m3)}_{i,x}W^k_{m3j}J^{k\tau s_z} \tag{35}$$

$$K^{k\tau sij}_{zx} = C^k_{36}N^{(n3)}_{j,y}W^k_{in3}J^{k\tau_z s} + C^k_{13}N^{(n1)}_{j,x}W^k_{in1}J^{k\tau_z s} + C^k_{45}N^{(m2)}_{i,y}N^{(n1)}_j W^k_{m2n1}J^{k\tau s_z} + C^k_{55}N^{(m1)}_{i,x}N^{(n1)}_j W^k_{m1n1}J^{k\tau s_z} \tag{36}$$

$$K^{k\tau sij}_{zy} = C^k_{23}N^{(n2)}_{j,y}W^k_{in2}J^{k\tau_z s} + C^k_{36}N^{(n3)}_{j,x}W^k_{in3}J^{k\tau_z s}_{y} + C^k_{44}N^{(m2)}_{i,y}N^{(n2)}_j W^k_{m2n2}J^{k\tau s_z} + C^k_{45}N^{(m1)}_{i,x}N^{(n2)}_j W^k_{m1n2}J^{k\tau s_z} \tag{37}$$

$$K^{k\tau sij}_{zz} = C^k_{33}W^k_{ij}J^{k\tau_z s_z} + C^k_{44}N^{(m2)}_{i,y}N^{(n2)}_{j,y}W^k_{m2n2}J^{k\tau s} + C^k_{45}N^{(m1)}_{i,x}N^{(n2)}_{j,y}W^k_{m1n2}J^{k\tau s} + C^k_{45}N^{(m2)}_{i,y}N^{(n1)}_{j,x}W^k_{m2n1}J^{k\tau s} + C^k_{55}N^{(m1)}_{i,x}N^{(n1)}_{j,x}W^k_{m1n1}J^{k\tau s} \tag{38}$$

References

[1] Carrera E. Historical review of zig-zag theories for multilayered plates and shells. Appl Mech Rev 2003;56(3):287–308.
[2] Carrera E. Theories and finite elements for multilayered, anisotropic, composite plates and shells. Arch Comput Methods Eng 2002;9(2):87–140.
[3] Kumar SK, Ganguli R, Harursampath D. Partial delamination modeling in composite beams using a finite element method. Finite Elem Anal Des 2013;76(0):1–12.
[4] Senthil K, Arockiarajan A, Palaninathan R, Santhosh B, Usha KM. Defects in composite structures: its effects and prediction methods *hata* A comprehensive review. Compos Struct 2013;106(0):139–49.
[5] Benvenuti E, Vitarelli O, Tralli A. Delamination of FRP-reinforced concrete by means of an extended finite element formulation. Compos Part B: Eng 2012;43(8):3258–69.
[6] Liu P, Xing L, Zheng J. Failure analysis of carbon fiber/epoxy composite cylindrical laminates using explicit finite element method. Compos Part B: Eng 2014;56(0):54–61.
[7] Banerjee S, Sankar BV. Mechanical properties of hybrid composites using finite element method based micromechanics. Compos Part B: Eng 2014;58(0):318–27.
[8] Carrera E. Theories and finite elements for multilayered plates and shells: a unified compact formulation with numerical assessment and benchmarking. Arch Comput Methods Eng 2003;10(3):215–96.
[9] Zhang Y, Yang C. Recent developments in finite element analysis for laminated composite plates. Compos Struct 2009;88(1):147–57.
[10] Yu W. Mathematical construction of a ReissnerâMindlin plate theory for composite laminates. Int J Solids Struct 2005;42(26):6680–99.
[11] Cinefra M, Carrera E. Shell finite elements with different through-the-thickness kinematics for the linear analysis of cylindrical multilayered structures. Int J Numer Methods Eng 2013;93:160–82.
[12] Mashat DS, Carrera E, Zenkour AM, Khateeb SAA, Filippi M. Free vibration of FGM layered beams by various theories and finite elements. Compos Part B: Eng 2014;59(0):269–78.
[13] Bletzinger KU, Bischoff M, Ramm E. A unified approach for shear-locking-free triangular and rectangular shell finite elements. Comput Struct 2000;75(3):321–34.
[14] Belytschko T, Tsay CS, Liu WK. A stabilization matrix for the bilinear mindlin plate element. Comput Methods Appl Mech Eng 1981;29(3):313–27.
[15] Panda SC, Natarajan R. Finite element analysis of laminated composite plates. Int J Numer Methods Eng 1979;14(1):69–79.
[16] Babuska I, Szabo B, Katz I. The *p*-version of the finite element method. SIAM J Numer Anal 1981;18(3):515–45.
[17] Hughes TJR, Cohen M, Haroun M. Reduced and selective integration techniques in the finite element analysis of plates. Nucl Eng Des 1978;46(1):203–22. special issue structural mechanics in reactor technology-smirt-4.
[18] Reddy JN. An evaluation of equivalent-single-layer and layerwise theories of composite laminates. Compos Struct 1993;25(14):21–35.
[19] Saravanos DA, Heyliger R, Hopkins DA. Layerwise mechanics and finite element for the dynamic analysis of piezoelectric composite plates. Int J Solids Struct 1997;34(3):359–78.
[20] Barbero EJ, Reddy JN. Modelling of delamination in composite laminated using a layer-wise plate theory. Int J Solids Struct 1991;28(3):373–88.
[21] Mitchell JA, Reddy JN. A refined hybrid plate theory for composite laminates with piezoelectric laminae. Int J Solids Struct 1995;32(16):2345–67.

[22] Mantari JL, Oktem AS, Soares CG. A new trigonometric layerwise shear deformation theory for the finite element analysis of laminated composite and sandwich plates. Comput Struct 2012;9495(0):45–53.
[23] Murakami H. Laminated composite plate theory with improved in-plane responses. J Appl Mech 1986;53(3):661–6.
[24] Cho M, Parmerter R. Efficient higher order composite plate theory for general lamination configurations. AIAA J 1993;31(7):1299–306.
[25] Cho M, Kim JS. Higher-order zig-zag theory for laminated composites with multiple delaminations. J Appl Mech 2000;68:869–77.
[26] Oh J, Cho M. A finite element based on cubic zig-zag plate theory for the prediction of thermo-electric-mechanical behaviors. Int J Solids Struct 2004;41(56):1357–75.
[27] Lee KH, Senthilnathan NR, Lim SP, Chow ST. An improved zig-zag model for the bending of laminated composite plates. Compos Struct 1990;15(2):137–48.
[28] Della CN, Shu D. Vibration of delaminated composite laminates: a review. Appl Mech Rev 2007;60(1):1–20.
[29] Zhou Z, Leung A, Xu X. The finite element discretized symplectic method for interface cracks. Compos Part B: Eng 2014;58(0):335–42.
[30] Oh J, Cho M, Kim J-S. Dynamic analysis of composite plate with multiple delaminations based on higher-order zigzag theory. Int J Solids Struct 2005;42(23):6122–40.
[31] Carrera E, Cinefra M, Nali P. MITC technique extended to variable kinematic multilayered plate elements. Compos Struct 2010;92(8):1888–95.
[32] Reissner E. The effect of transverse shear deformation on the bending of elastic plates. J Appl Mech 1945;12:69–76.
[33] Mindlin RD. Influence of rotatory inertia and shear in flexural motions of isotropic elastic plates. J Appl Mech 1951;18:28–31.
[34] Kirchhoff G. Uber das Gleichgewicht und die Bewegung einer elastishen Scheibe. Crelles J 1850;40:51–88.
[35] Bathe K-J, Chapelle Dominique. The finite element analysis of shells: fundamentals. Berlin: Springer; 2003.
[36] Bucalem ML, Bathe KJ. Higher-order MITC general shell elements. Int J Numer Meth Eng 1993;36:3729–54.
[37] Shen MHH, Grady JE. Free vibrations of delaminated beams. AIAA J 1992;30(5):1361–70.